Transport Properties of Metallic Ruthenates: A DFT + DMFT Investigation

Xiaoyu Deng,[1] Kristjan Haule,[1] and Gabriel Kotliar[1,2]
[1]Department of Physics and Astronomy, Rutgers University, Piscataway, New Jersey 08854, USA
[2]Condensed Matter Physics and Materials Science Department, Brookhaven National Laboratory, Upton, New York 11973, USA

(Received 1 April 2015; revised manuscript received 4 September 2015; published 20 June 2016)

We present a systematical theoretical study on the transport properties of an archetypal family of Hund's metals, Sr_2RuO_4, $Sr_3Ru_2O_7$, $SrRuO_3$, and $CaRuO_3$, within the combination of first principles density functional theory and dynamical mean field theory. The agreement between theory and experiments for optical conductivity and resistivity is good, which indicates that electron-electron scattering dominates the transport of ruthenates. We demonstrate that in the single-site dynamical mean field approach the transport properties of Hund's metals fall into the scenario of "resilient quasiparticles." We explain why the single layered compound Sr_2RuO_4 has a relative weak correlation with respect to its siblings, which corroborates its good metallicity.

DOI: 10.1103/PhysRevLett.116.256401

The transport properties of correlated materials are anomalous as they cannot be understood in terms of Fermi liquid (FL) theory [1], except at extremely low temperature. The term "bad metal" has been coined to stress their large resistivities that sometimes exceed the Mott-Ioffe-Regel limit [2]. Microscopic theoretical understandings of bad metals are slowly emerging. Dynamical mean field theory (DMFT) in simple Hubbard models [3,4], for example, explains the very low coherence scale T_{FL} below which strongly renormalized Landau quasiparticles are responsible for the transport. It also describes the transport properties at higher temperature, in terms of resilient quasiparticles with temperature-dependent mass renormalizations [5,6]. The bad metal behavior is commonly seen in a wide variety of correlated materials, such as cuprates [7,8], vanadates [9], ruthenates [10], nickelates [11], and organic metals [12]. While these materials all exhibit large resistivities, the magnitude and sometimes the temperature dependence of their resistivities are different. What the roles of various scattering processes are, e.g., electron-phonon coupling and electron-electron interaction, is not known *a priori*. Can the correlated nature of these materials, notably the local electron-electron interaction, account for their anomalous transport properties? What is the origin of the discrepancies if they exist? These open questions pose fundamental challenges to theoretical understanding and quantitative description of these materials. While DMFT seems to provide a promising avenue to investigate these issues, a solution requires systematic studies, which capture the effects of correlations and can be compared with comprehensive experimental measurements, on specific materials.

In this Letter we address the above issues in the Ruddlesden-Popper ruthenate family ($A_{n+1}Ru_nO_{3n+1}$), focusing on four metallic members: Sr_2RuO_4 ($n=1$), $Sr_3Ru_2O_7$ ($n=2$), $SrRuO_3$, and $CaRuO_3$ ($n=\infty$). Ruthenates have been extensively studied as prototype correlated systems, with large effective mass enhancements revealed by various experiments [13–26]. They exhibit a very small coherence scale T_{FL}, and a crossover into bad metal regime [10,26–30]. Surprisingly the single layered compound Sr_2RuO_4 is more metallic than the pseudocubic $SrRuO_3$ and $CaRuO_3$ at relative low temperature. This is different from many other systems, for example, the Ruddlesden-Popper family of strontium vanadates, lanthanum nickelates, lanthanum cuprates, strontium iridates, where the single layered compounds are insulating and the pseudocubic ones are metallic. In this Letter we investigate the correlated effects in these ruthenates, and demonstrate that the electron-electron interaction dominates their transport. We show that the relative weak correlation in Sr_2RuO_4 corroborates its good metallicity. Moreover, ruthenates are regarded as archetypal Hund's metals [31–35], in which Hund's interaction rather than the Hubbard repulsion gives rise to heavy quasiparticle mass. Our findings thus shed light on the scattering mechanism in Hund's metal and its consequence for the transport properties.

Our method is the combination of density functional theory and DMFT (DFT + DMFT), which is successful in the quantitative descriptions of electronic structures in many correlated systems [36]. We carry out the DFT + DMFT calculations in the charge self-consistent and all electron formulation, which avoids building the low energy Hubbard model, as implemented in Ref. [37] based on WIEN2k [38]. There are a few DFT + DMFT studies on ruthenates in the literature [31,39–41], but they are performed on low energy Hubbard models. Moreover, a complete investigation of the transport properties within a uniform DFT + DMFT scheme for these materials is missing.

We briefly introduce our calculation scheme and refer the details to Supplemental Material [42]. A large energy window 20 eV is used to construct the localized d orbitals, which permits us to use the same interaction parameters for

all the ruthenates. The Slater integrals within the localized orbitals are estimated to be $(F^0, F^2, F^4) = (4.5, 8.0, 6.5)$ eV, which amounts to $(U, J) = (4.5, 1.0)$ eV. We note that in previous studies [31,39–41] smaller interaction parameters are used, because there the local orbitals are constructed in a much smaller energy window thus more extended. The standard double counting in the fully localized limit form is adopted. The resistivity and optical conductivity are calculated using formalism of Ref. [37] in which the vertex corrections to the transport are neglected. The continuous-time quantum Monte Carlo method with hybridization expansion is used to solve the impurity problem [43,44]. Both polynomial fit and maximum entropy method are used to analytically continue the computed self energy. We focus on the paramagnetic states and neglect the ferromagnetism in $SrRuO_3$. We neglect the spin-orbit coupling effects.

We first justify our choice of interaction parameters by examining the effective mass enhancement, computed as $m^*_{\text{theory}}/m_{\text{DFT}} = 1/Z = 1 - (\partial \text{Re}\Sigma(\omega)/\partial\omega)|_{\omega=0}$. These values extracted at $T = 58$ K are presented in Table I, along with their experimental estimations. For $CaRuO_3$ and Sr_2RuO_4, they are in good agreement with experiments, and with previous DFT + DMFT calculations [31,39,40]. For $SrRuO_3$ no comparison is available since measurements are performed in the ferromagnetic state. Our result shows that the correlation strength of $SrRuO_3$ is close to that of $CaRuO_3$ despite the fact the latter has a larger distortion and slightly narrower bandwidth. The correlation is stronger in the considered paramagnetic phase than in the experimental ferromagnetic phase, which is expected since magnetism tends to reduce correlation. $Sr_3Ru_2O_7$ is peculiar with a strong momentum dependence of the effective mass enhancement revealed by quantum oscillation (QO) and angular-resolved photoemission spectroscopy (ARPES) [20,25]. Although the strong momentum dependence is beyond our single-site DMFT approach, our calculation gives a mass enhancement very close to the value (~6) on a large portion of the Fermi surface [25]. Since the theoretical mass enhancements across all the materials agree reasonably well with available experimental values, our current choice of parameters is satisfactory.

TABLE I. The mass enhancement of ruthenates in current DFT + DMFT calculations at $T = 58$ K. Values estimated from specific heat coefficients, ARPES, and quantum-oscillation measurements are presented for comparison. The experimental specific heat coefficients γ_{exp} are taken from Refs. [13–17], while the corresponding DFT values are computed with WIEN2k. $m^*_{\text{theory}}/m_{\text{DFT}}$ of $SrRuO_3$ and $CaRuO_3$ is averaged over t_{2g} orbitals. Note the $m^*_{\text{ARPES}}/m_{\text{DFT}}$ of $Sr_3Ru_2O_7$ is the value for a large fraction of the Fermi surface [25]. The $m^*_{\text{QO}}/m_{\text{DFT}}$ of $CaRuO_3$ is the value at zero magnetic field estimated in Ref. [26] assuming Kadowaki-Woods relation.

	Sr_2RuO_4	$Sr_3Ru_2O_7$	$SrRuO_3$	$CaRuO_3$
$(m^*_{\text{theory}}/m_{\text{DFT}})$	4.2 (xz/yz) 5.4 (xy)	6.3 (xz/yz) 6.4 (xy)	6.6	6.9
$(\gamma_{\text{exp}}/\gamma_{\text{DFT}})$	4	9	3.7 (FM)	6.5
$(m^*_{\text{ARPES}}/m_{\text{DFT}})$	≃3 [22,24]	≃6 [25]		
$(m^*_{\text{QO}}/m_{\text{DFT}})$	3, 3.5 (xz/yz) 5.5 (xy) [18]			6.1 [26]

The room temperature optical conductivities $\sigma(\omega)$ computed with DFT + DMFT are shown in Fig. 1, along with the experimental measurements and DFT predictions. Our results are consistent with the experiment measurements for all the compounds considered, and DMFT systematically improves the DFT results. The height and width of the Drude response are reasonably captured in our calculations. We note that the Drude response contains not only intraorbital but also interorbital transition among t_{2g} orbitals, which is argued to be important for the $\omega^{-1/2}$ behavior in $CaRuO_3$ [40]. A broad peak centered around 3 eV appears in all the compounds as observed in experiments. The broad peak is assigned to the transition between the O-2p to Ru-d orbitals. Note that DFT predicts an additional peak in $SrRuO_3$ at about 1.5 eV and in $CaRuO_3$ at about 2.0 eV, which can be assigned to t_{2g}-e_g transition. Its amplitude depends on the extent of $GdFeO_3$ distortion, and is insignificant or even

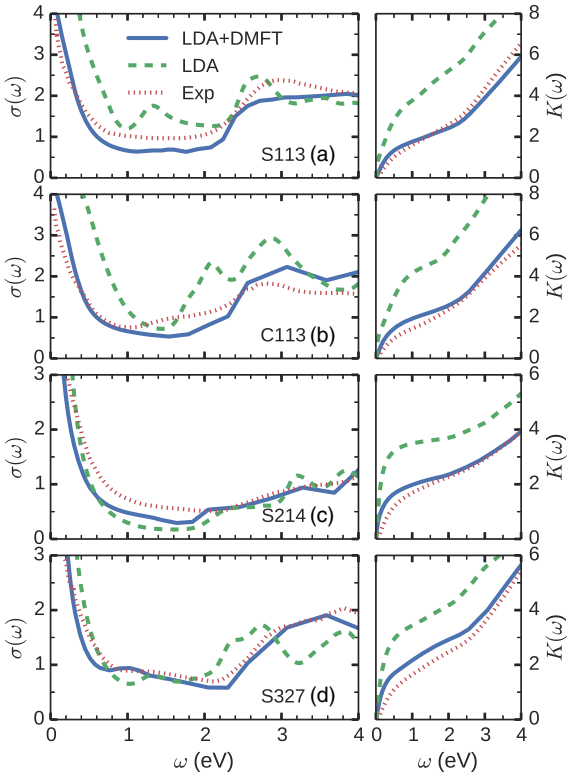

FIG. 1. The optical conductivity (left panel) and the corresponding integrated spectral weight (right panel) of ruthenates from DFT + DMFT ($T = 298$ K) and DFT calculations. Experimental data at room temperature are taken from [45] for comparison. S113 (a), C113 (b), S214 (c), and S327 (d) denote $SrRuO_3$, $CaRuO_3$, Sr_2RuO_4, and $Sr_3Ru_2O_7$ respectively.

missing in $Sr_3Ru_2O_7$ and Sr_2RuO_4, likely due to the matrix-element effects. However, this peak is shifted to higher frequency and merged with the broad peak at 3 eV in our DFT + DMFT results, in agreement with experiments.

The integrated spectral weight $K(\omega) = \int_0^\omega \sigma(\omega')d\omega'$, from both experimental and calculated optical conductivities, is depicted in Fig. 1. Strong correlations normally induce an anomalous spectral weight redistribution, which is the case in ruthenates. Compared with the DFT result, a significant reduction of $K(\omega)$ at low frequency is seen in the experimental data for all the ruthenates, and the spectral weight is transferred to higher frequency (≥ 4 eV). Our DFT + DMFT calculations capture the spectral weight reduction and the spectral weight redistribution of DFT band theory nicely for all the compounds. The good agreements between theory and experiments of both optical conductivity and spectral weight distribution are solid evidences that electron-electron correlations dominate the electron dynamics in ruthenates.

Now we focus on the resistivity of these compounds. The results are depicted in Fig. 2 and compared with experiments. We note that in our calculations the resistivity of $SrRuO_3$ ($CaRuO_3$) has a relative small anisotropy (less than 15%), in accordance with experimental determinations [46,47]; therefore, only the average over three principle axis is presented. For $CaRuO_3$ the agreement between the calculated and measured resistivity is almost perfect in both the overall scale and the temperature dependence in the whole temperature range. The shoulder at around 200 K that marks the substantial change of the slope of the resistivity is well captured. For $SrRuO_3$ the calculated resistivity is very close to that of $CaRuO_3$. Its agreement with experiment is very good above the Curie temperature $T_c \sim 160$ K; however, below T_c there is extra reduction of resistivity due to restoration of coherence in the ferromagnetic state, which is neglected in our calculations.

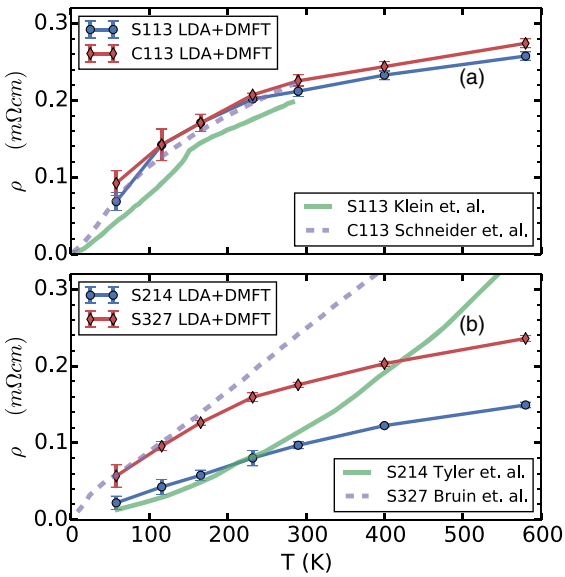

FIG. 2. The resistivity of ruthenates (a) $SrRuO_3$ and $CaRuO_3$, (b) Sr_2RuO_4 and $Sr_3Ru_2O_7$ calculated with DFT + DMFT, in comparison with the experimental measurements taken from [10,26,29,30]. The error bar is estimated from self energies of the last few converged iterations.

The agreement between the computed in-plane resistivities of the layered compounds Sr_2RuO_4 and $Sr_3Ru_2O_7$ and the experiments as shown in Fig. 2(b) is not as good as for $CaRuO_3$. The calculated resistivities have similar temperature dependence as those of the pseudocubic compounds with a shoulder at around 200–300 K. However, the measured ones are different. The resistivity of $Sr_3Ru_2O_7$ is almost linear in temperature up to 300 K with a weak shoulder showing up at low temperature (around 20 K), and that of Sr_2RuO_4 does not exhibit a shoulder at all. Nevertheless, there are three features correctly captured in our calculations. The resistivity of both compounds agrees reasonably in the overall scale with experiments, especially at relative low temperature. The resistivity shows no sign of saturation at high temperature, although the increasing is not as fast as found in experiments. And going from pseudocubic structure to layered structure, the material becomes more conductive.

Despite the difference in the coherence scale, the computed resistivity of ruthenates where Hund's coupling dominates the correlations has a very similar shape to that of the single band doped Hubbard model where Hubbard repulsion dominates the correlation [5]. Therefore, this anomalous shape is likely a characteristic of the resistivity in the single-site DMFT approach when the vertex corrections to the transport are neglected. The excellent agreement between the computed and the measured resistivities in $SrRuO_3$ and $CaRuO_3$, and the growing discrepancy in Sr_2RuO_4 and $Sr_3Ru_2O_7$, suggest that the vertex corrections have negligible contributions to the electron scattering in three-dimensional materials, but may play an increasingly important role in the quasi-two-dimensional systems. This is consistent with the fact that the vertex corrections are vanishing in large dimensionality [48,49]. The other possible source of discrepancies might be nonlocal interactions, which are not captured in our single-site DMFT approach. In addition we find that, in Sr_2RuO_4, the scattering due to the electron-phonon interaction is much smaller than that due to electron-electron interaction, by carrying out estimation of the electron-phonon coupling using the techniques of Ref. [50,51]. Therefore, electron-phonon interaction only accounts for a small fraction of the measured resistivity and the discrepancies between theory and experiment (see Supplemental Material [42]).

We note that in agreement with experiments, both Sr_2RuO_4 and $Sr_3Ru_2O_7$ exhibit strong anisotropy in our DFT + DMFT calculations that the calculated out-of-plane resistivity is orders of magnitude larger than the in-plane one. The large anisotropy comes from the anisotropy of the plasma frequency that is captured by DFT [52] and also presents in DFT + DMFT.

The relatively good metallicity of the layered compounds Sr_2RuO_4 with respect to its siblings is captured in our calculations. To gain more understanding we recall that the dc conductivity can be written as $\sigma = (\omega_p^*)^2\tau_{\rm tr}^*/4\pi$, where the effective plasma frequency ω_p^* and the effective scattering rate $1/\tau_{\rm tr}^*$ can be extracted from the computed optical conductivity [53]. As shown in Fig. 3, there is strong temperature dependence of ω_p^* and $1/\tau_{\rm tr}^*$ in all the compounds, which are characteristics of underlying resilient quasiparticles [53]. Interestingly unlike that of V_2O_3 in our previous study, $(\omega_p^*)^2$ in ruthenates shows a saturation (or weak temperature dependence) above $T \simeq 200$ K. This is possibly a characteristic of Hund's metal and needs to be justified in further studies. As discussed in Ref. [53], $(\omega_p^*)^2$ and $1/\tau_{\rm tr}^*$ are directly related to $1/Z$ and the quasiparticle scattering rate $\Gamma^* = -2Z{\rm Im}\Sigma(0)$, which have strong temperature dependences as shown in Fig. 4 for different orbitals. $1/Z$ s decrease when the temperature increases as found in previous studies [5,6,53], and interestingly all approach approximately 2 at high temperature. The temperature dependence of $1/Z$ is consistent with that of effective optical mass inferred from THz conductivity of $CaRuO_3$ [54]. In addition, both $1/\tau_{\rm tr}^*$ and Γ^* generally show hidden Fermi liquid behavior at relative low temperature such that they are approximately parabolic in temperature [6,53], although the behavior is elusive in $SrRuO_3$ [42]. Our results on the temperature dependence of $1/Z$ and Γ^* in $SrRuO_3$ and $CaRuO_3$ are consistent with a recent report using a different DFT + DMFT scheme [41]; however, the results on layered compounds and their connection to the transport properties are not available there.

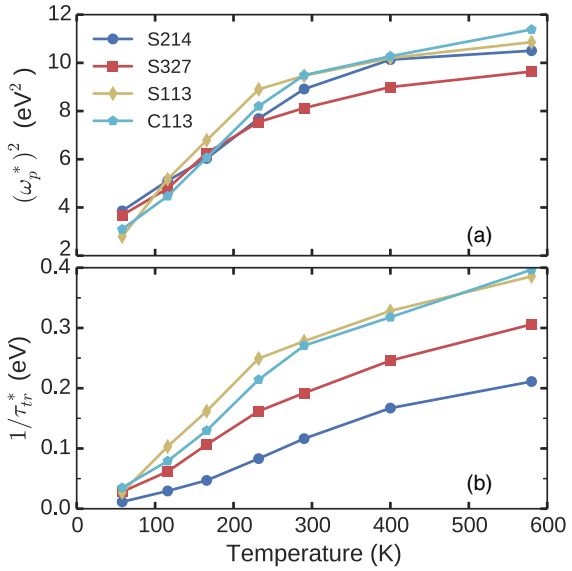

FIG. 3. The effective plasma frequency square $(\omega_p^*)^2$ (a) and the effective quasiparticle scattering rate $1/\tau_{\rm tr}^*$ (b) extracted from the computed optical conductivity with the DFT + DMFT method according to the formalism in Ref. [53].

Sr_2RuO_4 is the least correlated one in the ruthenates family according to the relative order of $1/\tau_{\rm tr}^*$. To understand the relative correlation strength in ruthenates, we look into the orbital-resolved quantities, the low temperature effective mass enhancement $m^*_{\rm theory}/m_{\rm DFT}$ in Table I, and the quasiparticle scattering rate Γ^* in Fig. 4(b). We find that the $d_{xz/yz}$ orbitals in Sr_2RuO_4 are the special ones with significantly smaller $m^*_{\rm theory}/m_{\rm DFT}$ and Γ^* than the others. The uniqueness of $d_{xz/yz}$ orbitals in Sr_2RuO_4 can be traced back to their one-dimensional nature. Because of quantum confinement by the Sr-O double layer along the out-of-plane axis, these orbitals have one-dimensional singularities at their band edges, and a low density of states near the Fermi level. The relative weak correlation strength in these orbitals can be understood within the same argument of Ref. [31], that the lower density of states ρ_F near the Fermi level implies stronger Weiss function in DMFT, ${\rm Im}\Delta(\omega \to 0) \simeq -(1/\pi\rho_F)$, and results in weaker correlation. We note that this argument holds because in ruthenates the real part of the local Green's functions ${\rm Re}G_{\rm loc}(\omega)$ is much smaller than the imaginary part ${\rm Im}G_{\rm loc}(\omega) = -\pi\rho_F$ near the Fermi level [42]. As n increases from Sr_2RuO_4 ($n = 1$), the density of states of $d_{xz/yz}$ orbitals near the Fermi level increases due to the relaxation of quantum confinement and the rotation of oxygen octahedra; therefore, the correlation is enhanced. Meanwhile orbital differentiation is reduced so that eventually the $d_{xz/yz}$ orbitals become nearly degenerate with the d_{xy} orbital in pseudocubic compounds and thus exhibit similar correlations. However, considering only d_{xy} orbitals (as well as $d_{xz/yz}$

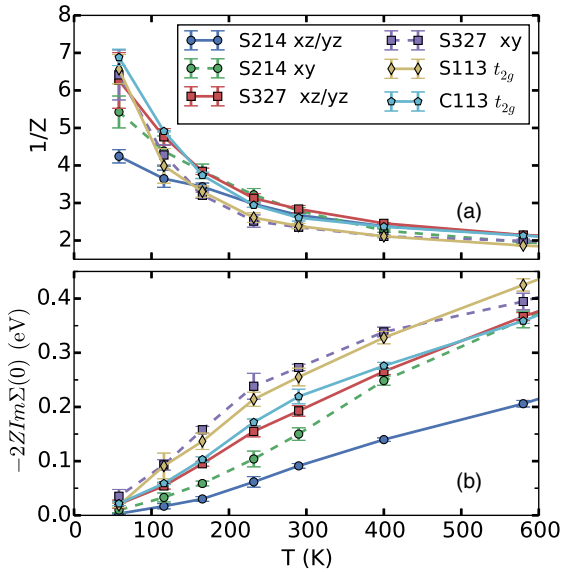

FIG. 4. The calculated effective mass enhancement $m^*_{\rm theory}/m_{\rm DFT} = 1/Z$ (a) and the effective quasiparticle scattering rate $\Gamma^* = -2ZIm\Sigma(0)$ (b) of different orbitals in ruthenates. The error bar is estimated from self energies of the last few converged iterations.

orbitals in pseudocubic compounds due to the near degeneracy), we find that their Weiss functions do not correlate with their relative correlation strength. Rather the effective mass enhancement in these orbitals is mostly related to the in-plane Ru-O bond length and the rotation of oxygen octahedra [42]. The d_{xy} orbital in Sr_2RuO_4 is slightly less correlated than the others because of the short in-plane Ru-O bond length and the absence of oxygen octahedron rotations in this compound. Our findings may shed light on the correlation effects in ruthenate thin films and heterostructures where the quantum confinement [55], the Ru-O bond length, and the distortions of oxygen octahedra could be engineered.

In conclusion, our study provides a quite accurate description of the transport properties in ruthenates and shows that they are dominated by electron-electron interactions. We demonstrate that the resilient quasiparticle scenario is valid in Hund's metals. We explain the origin of the relative good metallicity in Sr_2RuO_4. Our results also suggest that effects such as vertex corrections or nonlocal interactions need to be considered for more precise predictions of the resistivity of layered ruthenates.

We thank A. Georges and J. Mravlje for very useful discussions. We acknowledge support by NSF Grant No. DMR-1308141 (X. D. and G. K.) and NSF Grant No. DMR 1405303 (K. H.).

[1] P. Noziéres, *Theory of Interacting Fermi Systems* (Addison-Wesley, Reading, 1997).
[2] V. J. Emery and S. A. Kivelson, Phys. Rev. Lett. **74**, 3253 (1995).
[3] A. Georges, G. Kotliar, W. Krauth, and M. J. Rozenberg, Rev. Mod. Phys. **68**, 13 (1996).
[4] T. Pruschke, M. Jarrell, and J. K. Freericks, Adv. Phys. **44**, 187 (1995).
[5] X. Deng, J. Mravlje, R. Žitko, M. Ferrero, G. Kotliar, and A. Georges, Phys. Rev. Lett. **110**, 086401 (2013).
[6] W. Xu, K. Haule, and G. Kotliar, Phys. Rev. Lett. **111**, 036401 (2013).
[7] K. Takenaka, R. Shiozaki, S. Okuyama, J. Nohara, A. Osuka, Y. Takayanagi, and S. Sugai, Phys. Rev. B **65**, 092405 (2002).
[8] N. E. Hussey, K. Takenaka, and H. Takagi, Philos. Mag. **84**, 2847 (2004).
[9] H. Takagi, C. Urano, S. Kondo, M. Nohara, Y. Ueda, T. Shiraki, and T. Okubo, Mater. Sci. Eng. **63**, 147 (1999).
[10] A. W. Tyler, A. P. Mackenzie, S. NishiZaki, and Y. Maeno, Phys. Rev. B **58**, R10107 (1998).
[11] R. Jaramillo, S. D. Ha, D. M. Silevitch, and S. Ramanathan, Nat. Phys. **10**, 304 (2014).
[12] K. Takenaka, M. Tamura, N. Tajima, H. Takagi, J. Nohara, and S. Sugai, Phys. Rev. Lett. **95**, 227801 (2005).
[13] P. B. Allen, H. Berger, O. Chauvet, L. Forro, T. Jarlborg, A. Junod, B. Revaz, and G. Santi, Phys. Rev. B **53**, 4393 (1996).
[14] G. Cao, S. McCall, M. Shepard, J. E. Crow, and R. P. Guertin, Phys. Rev. B **56**, 321 (1997).
[15] M. Shepard, S. McCall, G. Cao, and J. E. Crow, J. Appl. Phys. **81**, 4978 (1997).
[16] Y. Maeno, K. Yoshida, H. Hashimoto, S. Nishizaki, S.-i. Ikeda, M. Nohara, T. Fujita, A. P. Mackenzie, N. E. Hussey, J. G. Bednorz, and F. Lichtenberg, J. Phys. Soc. Jpn. **66**, 1405 (1997).
[17] S.-I. Ikeda, Y. Maeno, S. Nakatsuji, M. Kosaka, and Y. Uwatoko, Phys. Rev. B **62**, R6089 (2000).
[18] C. Bergemann, A. P. Mackenzie, S. R. Julian, D. Forsythe, and E. Ohmichi, Adv. Phys. **52**, 639 (2003).
[19] C. S. Alexander, S. McCall, P. Schlottmann, J. E. Crow, and G. Cao, Phys. Rev. B **72**, 024415 (2005).
[20] A. Tamai, M. P. Allan, J. F. Mercure, W. Meevasana, R. Dunkel, D. H. Lu, R. S. Perry, A. P. Mackenzie, D. J. Singh, Z. X. Shen, and F. Baumberger, Phys. Rev. Lett. **101**, 026407 (2008).
[21] J. Mercure, S. K. Goh, E. C. T. O'Farrell, R. S. Perry, M. L. Sutherland, A. W. Rost, S. A. Grigera, R. A. Borzi, P. Gegenwart, and A. P. Mackenzie, Phys. Rev. Lett. **103**, 176401 (2009).
[22] H. Iwasawa, Y. Yoshida, I. Hase, K. Shimada, H. Namatame, M. Taniguchi, and Y. Aiura, Phys. Rev. Lett. **109**, 066404 (2012).
[23] D. E. Shai, C. Adamo, D. W. Shen, C. M. Brooks, J. W. Harter, E. J. Monkman, B. Burganov, D. G. Schlom, and K. M. Shen, Phys. Rev. Lett. **110**, 087004 (2013).
[24] C. N. Veenstra, Z. H. Zhu, B. Ludbrook, M. Capsoni, G. Levy, A. Nicolaou, J. A. Rosen, R. Comin, S. Kittaka, Y. Maeno, I. S. Elfimov, and A. Damascelli, Phys. Rev. Lett. **110**, 097004 (2013).
[25] M. P. Allan *et al.*, New J. Phys. **15**, 063029 (2013).
[26] M. Schneider, D. Geiger, S. Esser, U. S. Pracht, C. Stingl, Y. Tokiwa, V. Moshnyaga, I. Sheikin, J. Mravlje, M. Scheffler, and P. Gegenwart, Phys. Rev. Lett. **112**, 206403 (2014).
[27] G. Cao, W. Song, Y. Sun, and X. Lin, Solid State Commun. **131**, 331 (2004).
[28] N. E. Hussey, A. P. Mackenzie, J. R. Cooper, Y. Maeno, S. Nishizaki, and T. Fujita, Phys. Rev. B **57**, 5505 (1998).
[29] J. a. N. Bruin, H. Sakai, R. S. Perry, and A. P. Mackenzie, Science **339**, 804 (2013).
[30] L. Klein, J. S. Dodge, C. H. Ahn, G. J. Snyder, T. H. Geballe, M. R. Beasley, and A. Kapitulnik, Phys. Rev. Lett. **77**, 2774 (1996).
[31] J. Mravlje, M. Aichhorn, T. Miyake, K. Haule, G. Kotliar, and A. Georges, Phys. Rev. Lett. **106**, 096401 (2011).
[32] Z. P. Yin, K. Haule, and G. Kotliar, Nat. Phys. **7**, 294 (2011).
[33] Z. P. Yin, K. Haule, and G. Kotliar, Phys. Rev. B **86**, 195141 (2012).
[34] A. Georges, L. d. Medici, and J. Mravlje, Annu. Rev. Condens. Matter Phys. **4**, 137 (2013).
[35] K. Haule and G. Kotliar, New J. Phys. **11**, 025021 (2009).
[36] G. Kotliar, S. Savrasov, K. Haule, V. Oudovenko, O. Parcollet, and C. Marianetti, Rev. Mod. Phys. **78**, 865 (2006).
[37] K. Haule, C.-H. Yee, and K. Kim, Phys. Rev. B **81**, 195107 (2010).

[38] P. Blaha, K. Schwarz, G. K. H. Madsen, D. Kvasnicka, and J. Luitz, *WIEN2K An Augmented Plane Wave + Local Orbitals Program for Calculating Crystal Properties* (Karlheinz Schwarz, Techn. Universität Wien, Austria, Wien, Austria, 2001).
[39] E. Jakobi, S. Kanungo, S. Sarkar, S. Schmitt, and T. Saha-Dasgupta, Phys. Rev. B **83**, 041103 (2011).
[40] H. T. Dang, J. Mravlje, A. Georges, and A. J. Millis, Phys. Rev. Lett. **115**, 107003 (2015).
[41] H. T. Dang, J. Mravlje, A. Georges, and A. J. Millis, Phys. Rev. B **91**, 195149 (2015).
[42] See Supplemental Material at http://link.aps.org/supplemental/10.1103/PhysRevLett.116.256401 for the computational details, the estimation of resistivity induced by electron-phonon interaction, hidden Fermi liquid behavior, the Weiss function and local Green's functions, as well as the relation of correlation strength in d_{xy} orbital and structure parameters of ruthenates.
[43] K. Haule, Phys. Rev. B **75**, 155113 (2007).
[44] P. Werner, A. Comanac, L. de' Medici, M. Troyer, and A. J. Millis, Phys. Rev. Lett. **97**, 076405 (2006).
[45] J. S. Lee, Y. S. Lee, T. W. Noh, S. Nakatsuji, H. Fukazawa, R. S. Perry, Y. Maeno, Y. Yoshida, S. I. Ikeda, J. Yu, and C. B. Eom, Phys. Rev. B **70**, 085103 (2004).
[46] I. Genish, L. Klein, J. W. Reiner, and M. R. Beasley, Phys. Rev. B **75**, 125108 (2007).
[47] D. L. Proffit, H. W. Jang, S. Lee, C. T. Nelson, X. Q. Pan, M. S. Rzchowski, and C. B. Eom, Appl. Phys. Lett. **93**, 111912 (2008).
[48] A. Khurana, Phys. Rev. Lett. **64**, 1990 (1990).
[49] S. T. F. Hale and J. K. Freericks, Phys. Rev. B **83**, 035102 (2011).
[50] S. Y. Savrasov and D. Y. Savrasov, Phys. Rev. B **54**, 16487 (1996).
[51] X. Gonze *et al.*, Comput. Phys. Commun. **180**, 2582 (2009).
[52] D. J. Singh, Phys. Rev. B **52**, 1358 (1995).
[53] X. Deng, A. Sternbach, K. Haule, D. N. Basov, and G. Kotliar, Phys. Rev. Lett. **113**, 246404 (2014).
[54] S. Kamal, J. Dodge, D.-M. Kim, and C. B. Eom, in *Quantum Electronics and Laser Science Conference, 2005, QELS '05* (IEEE, Baltimore, 2005), pp. 443–445.
[55] Y. J. Chang, C. H. Kim, S. H. Phark, Y. S. Kim, J. Yu, and T. W. Noh, Phys. Rev. Lett. **103**, 057201 (2009).